PAPER

Check for updates

Supramolecular biomaterials as drug nanocontainers with iron depletion properties for antimicrobial applications†

Chiara Zagni, [ID] [a] Vincenzo Patamia, [ID] [a] Sandro Dattilo, [b] Virginia Fuochi, [c] Salvatore Furnari, [c] Pio Maria Furneri, [c] Sabrina Carola Carroccio, [ID] ‡ [b] Giuseppe Floresta [ID] * [a] and Antonio Rescifina [ID] ‡ [a]

This work reports the design of a new bacteria-killer based on maltol derivatives and β-cyclodextrin cryogels. The maltol covalently linked to the 3D polymer network chelates the iron ions efficiently, subtracting them from the bacterial environment, thus impeding microbial survival. At the same time, the hydrophobic cavities of β-cyclodextrin can work as nanocontainers to release pharmaceuticals on the infected tissue, reinforcing the bactericidal action. This non-conventional dual-acting system was successfully tested with and without the complexation of lomefloxacin by β-cyclodextrin. The material's remarkable activity was proven on Gram-positive and Gram-negative bacteria. As it turns out, such material is bactericidal owing to maltol chelating features; moreover, the material is able to improve the bactericidal activity when it releases lomefloxacin after its complexation inside β-cyclodextrin. Indeed, the presence of β-cyclodextrin nanocontainers holds the promise of compliance with various drugs, opening up exciting possibilities for diverse therapeutic applications. These innovations could potentially bring a new vista to wound dressing.

Introduction

The discovery of new antibacterial action models for medications is a health challenge of the highest relevance in the age of rising antimicrobial resistance.[1] One of the strategies to ensure progress consists of increasing or enhancing the chelating properties of already-existing medications.

Indeed, metal-chelating agents exhibit antibacterial action by disrupting the microorganism's vital metal metabolism and obstructing metal uptake and bioavailability for critical reactions.[2] The biological function of metal-dependent proteins, such as metalloproteases and transcription factors, can be inhibited by the chelation activity, which disturbs the homeostasis of microbial cells and blocks microbial nutrition,

growth, and development, cellular differentiation, adhesion to biotic (such as extracellular matrix components, cells and/or tissues) and abiotic (such as plastic, silicone, and acrylic) structures, as well as the *in vivo* infection. It is worth noting that chelating drugs also increase the effectiveness of traditional antibacterial substances.[2–4] Designing new naturally inspired chelating agents can be a promising approach to overcoming antimicrobial resistance.[5] Resistance-based infections frequently do not respond to standard treatment, prolonging sickness, increasing their cost, and raising the chance of mortality. Since the current antimicrobial medications either have many adverse effects or tend to lose their efficacy owing to the selection of resistant strains, the design of innovative antimicrobial treatments is becoming more and more challenging.[6] This evidence led to several new techniques for impeding crucial biological processes in microbial cells.

Nano-molecular structuration has all the characteristics to cope with such constraints, creating novel systems that are able to target bacterial infections more effectively. Their distinctive hydrophobic/hydrophilic architectures enable loading various medications in relatively high quantities, improving their solubility and safeguarding them against deterioration.[7–9] Nanocontainers have found extensive applications in wound healing owing to their exceptional abilities in adsorption, drug loading, and antimicrobial properties.[10] An ideal wound dressing should encompass more than solely antibacterial capabilities.

[a] Department of Drug and Health Sciences, University of Catania, V.le A. Doria 6, 95125, Catania, Italy. E-mail: giuseppe.floresta@unict.it

[b] Institute for Polymers, Composites, and Biomaterials, CNR-IPCB, Via Paolo Gaifami 18, 95126, Catania, Italy

[c] Department of Biomedical and Biotechnological Sciences (Biometec), University of Catania, Via S. Sofia 89, 95125, Catania, Italy

It should possess biocompatibility and biodegradability, effectively retain moisture, facilitate oxygen permeation, aid in exudate removal, safeguard the wound against pathogens and physical irritation, enhance cellular responses, and actively contribute to wound healing. In this regard, three-dimensional (3D) network polymers such as hydrogels or cryogels are widely used.[11]

These materials exhibit significant potential for application in biological contexts due to their ability to (i) mimic the three-dimensional environment of the extracellular matrix, (ii) facilitate drug loading with assured sustained release,[12] (iii) serve as medical dressings owing to their high biocompatibility and flexibility, effectively mitigating additional patient injuries caused by wound adhesion[13,14] and (iv) enhance treatment effectiveness by enabling the least intrusive delivery of cells or biomolecules to patients.[15]

Thanks to their large and interconnected pores, cryogels are characterized by superior mechanical and swelling properties.[16] The literature reports highly porous cryogels made of poly(2-hydroxyethyl methacrylate) (pHEMA) and poly(tannic acid) (pTA)[17] as antimicrobial materials for wound dressing. Similarly, poly(hydroxyethyl methacrylate)-N-methacryloyl-(L)-histidine methyl ester (pHEMA-MAH) based cryogel membranes imprinted with lysozyme were reported to be innovative materials based on α/β/γ-cyclodextrin (α/β/γ-CD) that has been co-polymerized with 2-hydroxyethyl methacrylate (HEMA) to obtain 3D macroporous cryogels with hydrophobic cavities,[18] which have been successfully loaded with different drugs achieving an impressive drug loading efficiency (DLE). It was demonstrated that the presence of CDs within cryogels benefits loading capacity and drug delivery.[19]

In this forward-looking context, we designed a novel drug delivery system combining CD and the maltol derivative properties. *Via* a one-pot cryo-polymerization, the components – HEMA, β-CD acrylate, and maltol derivative – react to generate a cutting-edge cryogel material with remarkable antibacterial potential. Our main objective is to develop a wound dressing that exploits an innovative approach to explicate antibacterial properties and can, in addition, encapsulate therapeutic agents.
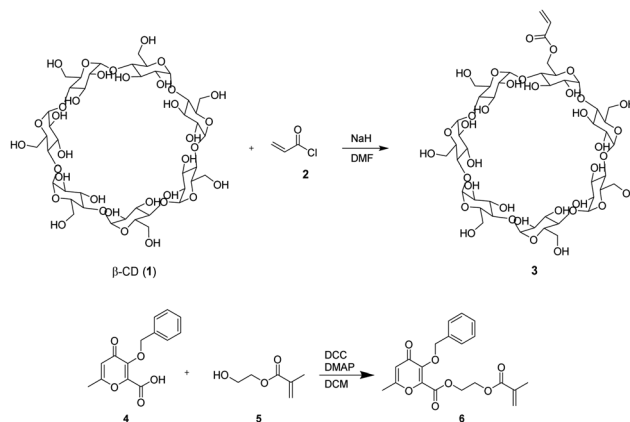

Fig. 1 Synthesis of monomers **3** and **6**.

The comonomer maltol derivative **6** was synthesized by a condensation reaction involving benzylated maltol derivative **4** and HEMA in the presence of DCC and DMAP (Fig. 1). The successfulness of the synthesis was verified by NMR spectroscopy, as reported in the experimental section. The molecule's characteristic signals are present in both the ^{1}H NMR and the ^{13}C NMR spectra. Monomers **3** and **6** were mixed with HEMA and underwent radical cryo-polymerization at –15 °C in the presence of N,N′-methylenebisacrylamide (MBAA) as a cross-linker. The reaction started after adding ammonium persulfate (APS) and tetramethylethylenediamine (TEMED) (Fig. 2). Cryogel **7** was treated with TFA to remove benzylic groups, generating the final product **8**.

The morphology of sample **8** was observed using scanning electron microscopy, shown in Fig. S1 (ESI†). The synthesized material exhibits a characteristic macroporous structure with an average pore size of 25 μm, as determined by pore size distribution analysis (see the ESI†). The highly porous network within the scaffold facilitates both adsorption and drug release processes in a wet environment.

Swelling properties were determined by the standard gravimetric procedure.[8] Cryogel β-CD/HEMA/Malt exhibited a slightly higher swelling ratio than β-CD/HEMA and lower than HEMA cryogels (Fig. S2a, ESI†). This observation can be

Results and discussion

Due to their tunable chemistry, pore architecture, water uptake capacities, and flexibility, cryogels are excellent candidates for our purpose.[20] In this view, biobased cryogels were synthesized starting from naturally occurring molecules: β-cyclodextrin **1** and the maltol derivative **4**. In fact, while maltol and its derivatives are recognized for their well-established iron-chelating properties,[21,22] β-cyclodextrin stands out as one of the most frequently employed to form inclusion complexes with hydrophobic drugs. Functionalization of β-cyclodextrin by reaction with acryloyl chloride **2** was carried out to initiate the cryo-polymerization process.
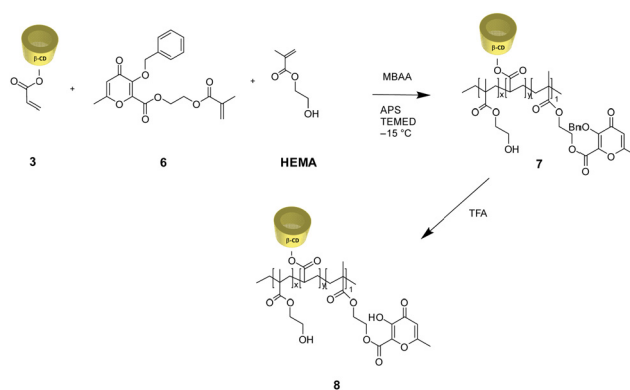

Fig. 2 Schematic representation of β-CD/HEMA/Malt (**8**) cryogel synthesis.

reasonably attributed to the abundant cross-linking moieties in the functionalized cyclodextrin, influencing absorption properties while the maltol portion marginally increases the water uptake capacity.

To evaluate its thermal stability, β-CD/HEMA/Malt cryogel (**8**) was characterized by thermogravimetric analyses (TGA). The thermogram shown in Fig. S2b (ESI†) confirmed good thermal stability with a single degradation step. The maximum degradation rate is at 456 °C and corresponds to the simultaneous degradation of the polymeric architecture and the cyclodextrin structure. Fourier transform infrared (FTIR) spectroscopy confirmed the success of the polymerization reaction. Fig. S3 (ESI†) shows the IR spectra of compounds **6–8**. For compound **6**, the 2931 cm^{-1} stretching related to C–H and the two very intense C=O streaks, related to the α,β-unsaturated ester and ketone, at 1726 and 1654 cm^{-1}, respectively, are visible. Also characteristic of monomer **6** are the 1242 cm^{-1} signals attributable to the stretching of the ether group and the 735 cm^{-1} bending of the aromatic C–Hs.[23–25] In compound **7**, both the signals related to compound **6** and those typical of cryogels prepared with HEMA as a monomer are visible, *i.e.*, O–H stretching between 3100 and 3800 cm^{-1} and C–H stretching between 2870 and 3000 cm^{-1},[19] which overlap with those of compound **6**. In

Table 1 Fe(III) retention percentage of β-CD/HEMA/Malt cryogels

Fe(III) C_0 (mg L^{-1})[a]	Fe(III) C_e (mg L^{-1})[b]	Fe(III) retention (%)
1.70	0.04	97.64
7.00	0.73	89.57

[a] C_0 is the initial concentration. [b] C_e is the final concentration.

molecule **8**, conversely, due to the debenzylation reaction, the signals at 1242 and 735 cm^{-1}, related to benzyl ether and aromatic C–Hs, are absent. The main antimicrobial activity of the β-CD/HEMA/Malt cryogel relies on its iron-chelating ability. To evaluate it, cryogels **7** and **8** were immersed in a solution containing Fe(III). Fig. 3a highlights that the β-CD/HEMA/Malt cryogel (**8**) effectively sequestered iron ions, causing the chromatic change of the solution from orange to colorless. ICP/MS analysis was performed to estimate the solution's residual Fe(III) amount. Fig. 3b reports the chelation kinetic profile measured in ppm after reaching adsorption/desorption equilibrium. The experiments were carried out at different iron concentrations to test the chelating capacity of the cryogel. Cryogel **8** sequestered almost all the metal in the solution at an iron concentration of 1.7 ppm, whereas at 7 ppm, the material chelated about 90% of it (Table 1). This value (6.27 mg L^{-1}) corresponds to the maximum iron amount that can be adsorbed in such conditions.

To expand the cryogel's therapeutic potential, we strategically introduced β-cyclodextrin into the polymeric structure, creating a versatile platform for drug loading. This innovative approach allowed us to exploit the cryogel's dual functionality; iron cations can be effectively captured to exert antimicrobial effects, and simultaneously, drugs can be loaded to include a synergistic antibacterial activity. It was previously demonstrated that β-CD/HEMA cryogel could load different drugs.[19] Among them, lomefloxacin (LOM) was particularly interesting since it has been used for treating various bacterial infections.[19] After the synthesis, β-CD/HEMA and β-CD/HEMA/Malt (**8**) cryogels were dried, cut into small slices of the same weight and diameter, and loaded with a small amount of LOM. The amount of drug loaded into the sponge-like material **8** was determined using UV-vis spectroscopy (see the ESI†). This value ranges from 65% to 70%, with slight differences between **8** and β-CD/HEMA, used as reference (Fig. 4a).
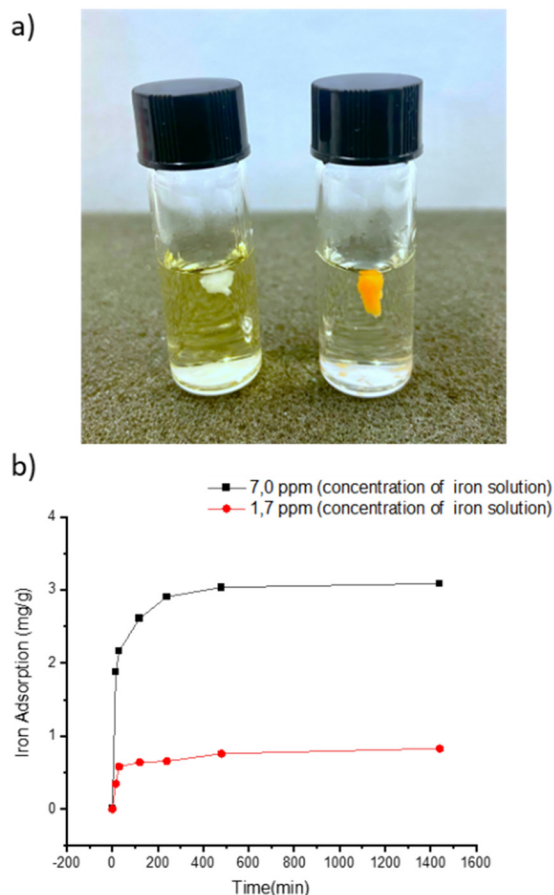

Fig. 3 (a) Representative picture of the cryogel immersed in FeCl$_3$ solution (β-CD/HEMA/Malt (**8**) on the left and β-CD/HEMA on the right); (b) iron adsorption kinetic of β-CD/HEMA/Malt cryogel (**8**).
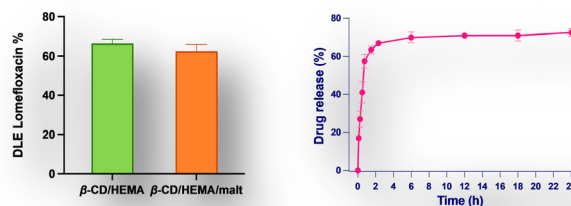

Fig. 4 (a) Drug loading efficiency of lomefloxacin (LOM) for β-CD/HEMA and β-CD/HEMA/Malt cryogels (**8**). (b) Drug release of LOM from β-CD/HEMA/Malt cryogels (**8**).

The release of the drug from the cryogel was investigated by soaking a weighted portion of the sponge in phosphate saline buffer at pH = 7.4. The amount of pharmaceuticals released was calculated by measuring the absorbance of the solution (Lomefloxacin titration curve obtained by UV spectroscopy, Fig. S4 (ESI†), Fig. 4b). As expected,[26] the drug is released gradually over time, with an initial burst effect and a sustained release lasting up to 24 h. After this time, the equilibrium was achieved with a drug release (desorption) that reached 71%. The LOM kinetic release was described using zero order, first order, Higuchi, Weibull, and Korsmeyer–Peppas models (Fig. S7, ESI†). The Weibull model was found to have the best fit (R^2 value of 0.99) among the other equations tested. This finding suggested that the rapid dissolution of the LOM adsorbed at the surface caused the initial burst effect, while its sustained release depends on molecules inserted into CD cavities.[23]

Cryogel **8** was tested against *Staphylococcus aureus*, *Pseudomonas aeruginosa*, and *Klebsiella pneumoniae* pathogens to evaluate its potential antibacterial activity. Experiments were carried out without charging LOM into the cryogel **8**. As shown in Fig. 5, the results confirm a remarkable antibacterial activity toward the pathogens tested with an MIC value of 3.0 mg mL^{-1}. This was also the value for the MBC, showing that cryogel **8** had bactericidal activity at the same concentration. Notably, the relevant antibacterial effectiveness is exclusively ascribable to the iron-depletion property of the maltol derivative included in **8**. As shown in the bacterial growth curves (Fig. 5), antibacterial action was noticeable in Gram-positive and Gram-negative strains.

As shown from the disk diffusion test, this effect is more pronounced against *K. pneumoniae*, confirming the higher iron demand of these bacteria (Fig. 6 and Table 2). Conversely, β-CD/HEMA cryogel did not show any activity since neither chelating nor pharmaceutical activity can be imputable to the compound. As expected, antibacterial activity was clearly manifested when LOM was added to β-CD/HEMA. The activity is lower than the reference (10 µg) since the final drug release was assessed at approximately 4.5 µg (Fig. 6). It is important to note that even if the inhibition results of **8** loaded with LOM compared to the reference may appear similar, the concentration of LOM inside the cryogels **8** is significantly lower than the reference. This can be deduced from the DLE of 63% and drug release of around 70% (Fig. 4). Even though the cryogel **8** releases 50% less drug, it still produces an equivalent inhibition halo as 10 µg of LOM.

Finally, a cell viability assay was performed on the H1HeLa cell line to assess the potential cytotoxicity in human cells. The results showed that the cryogel (**8**) did not exhibit cytotoxicity effects at 3.0 and 6.0 mg (Fig. 7).
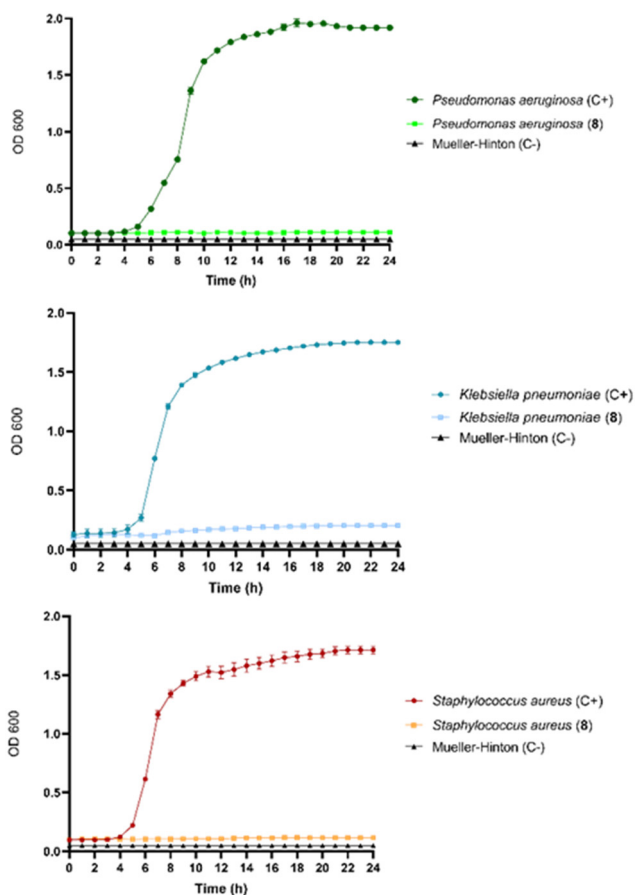

Fig. 5 Growth inhibition curves analysis of *Pseudomonas aeruginosa* ATCC 27853, *Klebsiella. pneumoniae* ATCC 700603, and *Staphylococcus aureus* ATCC 29213 in the presence of cryogel **8**. All experimental data were expressed as mean ± SD. C+ (positive control, growth of the *bacterium* without drugs); C− (negative control, only Müller–Hinton broth).

Experimental

Materials

β-CD, acryloyl chloride, maltol, sodium hydride in mineral oil (69%), acetone, dimethylformamide anhydrous (DMF), 2-hydroxyethyl methacrylate (HEMA), *N,N'*-methylene-bisacrylamide (MBAA), ammonium persulfate (APS), tetramethyl-ethylene-diamine (TEMED), trifluoroacetic acid (TFA), FeCl$_3$ and Lomefloxacin (LOM) were purchased from Merck. A Milli-Q water purification system was used to produce deionized water.
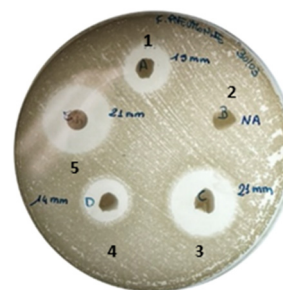

Fig. 6 Agar disk diffusion method over *K. pneumoniae*: (1) β-CD/HEMA + LOM, (2) β-CD/HEMA, (3) β-CD/HEMA/Malt (**8**) + LOM, (4) β-CD/HEMA/Malt (**8**) and (5) LOM.

Table 2 Antimicrobial activity of cryogels against bacterial pathogens. Results were expressed in mm (mean ±SD). Values less than 6 mm indicate no activity

Pathogens	β-CD/HEMA + LOM	β-CD/HEMA	8 + LOM	8	LOM 10 mg
S. aureus	23.5 ± 1.0	<6	24.0 ± 1.0	<6	25.0 ± 1.0
E. faecalis	13.5 ± 0.5	<6	13.0 ± 0.5	<6	23.0 ± 1.0
P. aeruginosa	13.0 ± 0.5	<6	14.0 ± 0.5	<6	23.5 ± 1.0
E. coli	30.0 ± 0.5	<6	32.0 ± 1.0	<6	29.0 ± 0.5
K. pneumoniae	14.0 ± 1.0	<6	21.5 ± 1.0	15.0 ± 1.0	22.0 ± 1.0

Synthesis

Synthesis of β-CD-acrylate monomer (3). β-CD (**1**) (1 g, 1.0278 mmol) was dissolved in DMF (14 mL) in a round-bottom flask under nitrogen and NaH (164.6 mg, 4.1116 mmol, 4 eq.) was added at 0 °C and the reaction mixture was stirred for 1 h. After that, acryloyl chloride (**2**) (171 mL, 4.1116 mmol, 4 eq.) was added dropwise.[19,27] The reaction was carried out for 24 h at r.t. with stirring. Then, it was poured into a rotavapor to concentrate the solution. Cold acetone was added, and the solid was recovered by filtration and dried for 24 h in a drying oven. Yield 85%. ^{1}H NMR (reported in Fig. S5, ESI†) (500 MHz, DMSO-d$_6$): δ = 6.43–6.03 (m, 4H), 5.99–5.76 (m, 2H), 5.72–5.34 (m, 12H), 4.88–4.70 (m, 6H), 4.66–4.33 (m, 8H), 3.85–3.71 (m, 7H), 3.69–3.56 (m, 16H), 3.31–3.24 (m, 6H); ^{13}C NMR (reported in Fig. S6, ESI†) (126 MHz, DMSO-d$_6$): δ = 165.67, 130.62, 101.87, 82.09, 73.28, 72.12, 60.03, 35.82, 33.93, 30.80.[19,28]

Synthesis of Malt monomer (6). Molecule **4** was synthesized as reported in the literature.[22] 60 mg of DCC (0.288 mmol), 28 mg of DMAP (0.230 mmol) and 24 μL of HEMA (**5**) (0.192 mmol) were added to 50 mg of 3-(benzyloxy)-6-methyl-4-oxo-4H-pyran-2-carboxylic acid (**4**) (0.192 mmol) in DCM (2 mL) and the reaction was magnetically stirred at room temperature overnight. After this time, the reaction crude was filtered off, and the solution was washed with a saturated solution of NaHCO$_3$ (3 × 2 mL) and then with brine (3 × 2 mL). Finally, the organic phase was dried over Na$_2$SO$_4$ and evaporated under vacuum to obtain a light-yellow oil. Yield 60%. ^{1}H NMR (500 MHz, CDCl$_3$): δ = 7.48–7.44 (m, 2H), 7.35–7.30 (m, 3H), 6.27 (s, 1H), 6.11 (s, 1H), 5.57–5.56 (m, 1H), 5.30 (s, 2H), 4.52–4.51 (m, 2H), 4.38–4.37 (m, 2H), 2.31 (s, 3H), 1.92

(s, 3H). ^{13}C NMR (126 MHz, CDCl$_3$): δ = 176.64, 167.09, 165.32, 159.98, 148.25, 145.17, 136.41, 135.87, 128.91, 128.56, 128.49, 126.42, 115.67, 74.61, 63.83, 62.03, 19.91, 18.35.

Synthesis of β-CD/HEMA/Malt cryogel (8). Compounds **3**, **5**, and **6** in a weight ratio of 1 : 2 : 1 were added to 1 mL deionized water and mixed. The solution was kept in an ice bath, and after that, APS and TEMED, at a final concentration of 1.5%, were added. The mixture was poured into 5 mL plastic syringes with a 1.2 cm diameter and stored at −17 °C for 24 hours. In order to compare the results, pure β-CD/HEMA cryogels were also synthesized. All cryogels were cleaned with distilled water to remove impurities after the polymerization. The polymerization yield was 86%. **7** (50 mg) was suspended in TFA (2 mL) for 12 h at r.t. TFA was removed, and the final product **8** was washed with water (3 × 10 mL). β-CD/HEMA was also synthesized as a reference following the previously described procedure.

NMR spectroscopy

^{1}H and ^{13}C NMR spectra were recorded at 300 K using a Varian UNITY Inova, at 500 MHz for ^{1}H NMR and 125 MHz for ^{13}C NMR. Chemical shift (δ) values are given in ppm.

Fourier transform infrared (FTIR)

FTIR spectra in the 4000–400 cm^{-1} region were obtained using an FTIR System 2000 (PerkinElmer, Waltham, MA, USA) and KBr as media to determine the functional groups of the cryogels.

Thermogravimetric analysis (TGA)

Thermal stability and kinetics parameters of the synthesized materials were determined using the TA instruments operating software. The measurements were performed in a temperature range of 40 °C to 800 °C, at a heating rate of 10 °C min^{-1} under nitrogen flow (60 mL min^{-1}), using 5 ± 0.1 mg of sample. The weight loss percentage was determined by TGA.

Scanning electron microscopy (SEM)

Surface morphologies of cryogel samples were observed using a desktop scanning electric microscopy Thermo Phenom Prox (Thermo Fisher Scientific – Waltham, MA, USA) (SEM) combined with a fully integrated energy-dispersive X-ray detector (Silicon Drift Detector). Dried samples were cut into thin discs (1–2 mm thick) and sputtered with gold (<10 nm) to confer conductivity. The data were acquired and processed using Phenom Porometric 1.1.2.0 (Phenom-World BV, Eindhoven,
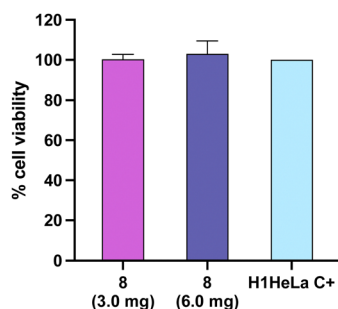

Fig. 7 The survival assay in human cell line H1HeLa with 3.0 and 6.0 mg of cryogel **8**. Bars represent the mean ± SD of three independent experiments (C), *E. coli* (D), and *K. pneumoniae* (E). β-CD/HEMA + LOM (1), β-CD/HEMA (2), **8** + LOM (3), **8** (4) and LOM (5).

The Netherlands). Porosimetric distribution was calculated with SEM Porometric software (Thermophenom).

Swelling test

Each cryogel was precisely sectioned into small specimens measuring 9 mm in diameter and 10 mm in length. These samples were immersed in excess deionized water to ensure thorough removal of any unreacted monomers, initiators, or soluble polymers. The water was changed twice daily until the samples reached a swelling equilibrium at room temperature. Before weighing, each sample was carefully removed from the water, and any surface water was gently blotted. To ensure precision, each sample was weighed at least three times. Subsequently, the swollen samples were subjected to freeze-drying and weighed again. The entire procedure was conducted with three parallel samples for each type of cryogel, and the average result was computed with a standard deviation consistently below 5%.

Drug loading

Lomefloxacin (LOM) was dissolved in water at a concentration of 0.1 mg mL^{-1}. Then, 100 μL of each solution was loaded into 2 mg of dried cryogel (**8**). The samples were incubated for 24 h in the dark. Then, the sample was washed with water. Aqueous wastes were collected to estimate the real loading capacity by measuring the amount of drug discharged using a UV-Vis spectrophotometer. Subsequently, the drug-loaded cryogels were frozen and freeze-dried for 24 h. The tests were performed in triplicate.

The following equation was used to calculate drug loading efficiency (DLE) or drug loading content.[19]

$$\mathrm{DLE}(\%) = \frac{\text{Weight of loaded drug}}{\text{Weight of total drug}} \times 100$$

Drug release

Drug-loaded freeze-dried cryogels were tested for drug release in phosphate saline buffer (PBS, pH 7.4) at 37 °C. Each sample was placed in a vial with 10 mL of saline buffer, and various aliquots were taken at various intervals: 10 and 30 minutes, 1, 2, 3, 4, 5, 8, and 24 hours. The released amount of lomefloxacin was determined using a UV-Vis JASCO spectrophotometer based on the calibration curves of the drug in the specific medium (Fig. S1, ESI†) in a concentration scale of 0.01–0.05 mg mL^{-1}. The tests were performed in triplicate.

Drug release efficiency (DRE) was calculated from the following equation:

$$\mathrm{DRE}(\%) = \frac{\text{Mass released drug}}{\text{Mass loaded drug}} \times 100$$

Kinetics model of release

The release behavior of β-CD/HEMA/Malt cryogel has been investigated using Prism software to calculate the coefficient of determination (R) and fit with the mathematical models used in drug delivery. The linearized formulations of zero-order and first-order kinetics of the Korsmeyer–Peppas, Higuchi, and Weibull models used to evaluate the kinetic release parameters are described in the equations below.

Zero-order kinetics:

$$M_t/M_\infty = k_0 t$$

this kinetic expresses a constant release over time, often related to solid dissolution.[29]

First-order kinetics:

$$M_t/M_\infty = 1 - e^{-k_1 t}$$

In this case, the drug release is concentration-dependent; thus, it decreases with time.[30]

Korsmeyer–Peppas model:

$$M_t/M_\infty = k_3 t^n$$

this equation has been designed to describe drug release from polymeric matrix systems.[31]

Higuchi model:

$$M_t/M_\infty = k_3 t^{\frac{1}{2}}$$

this represents one of the most used models for drug release from matrix devices.[32]

Weibull model:

$$M_t/M_\infty = 1 - \exp(-a t^b)$$

helpful in fitting the drug release by nanosystems.[33]

The amount of drug injected into the system at time 0 is represented by M_∞ in all the equations. M_t represents the cumulative release at time t, and the release time is represented by t, while n, a, and b are specific indices.

ICP/MS

Quantitative determination of iron ions in solution was performed using an inductively coupled plasma–mass spectrometry (ICP/MS) Nexion 300X (PerkinElmer Inc. Waltham, Massachusetts, USA.) instrument using the kinetic energy discrimination (KED) for interference suppression. Each determination was performed three times. The accuracy of the analytical procedure was confirmed by measuring a standard reference material, Nist 1640a trace element in natural water, without observing an appreciable difference. Batch equilibrium tests were carried out to calculate the metal ions removal percentage. In general, 10 mg of cryo-sponges were immersed into iron(III) chloride (FeCl$_3$) solutions (5 mL at pH = 6) at different initial concentrations of 1.7 and 7 mg L^{-1} as Fe content. The vials were maintained under constant shaking at 25 °C and 180 rpm for 24 h, withdrawing aliquots of 100 μL at different intervals. The residual metal ion concentrations were evaluated by ICP-MS measurements.

Antibacterial activity

Inhibitory activity of β-CD/HEMA/Malt cryogel (**8**) was measured against *Escherichia coli* ATCC 25922, *Klebsiella pneumoniae* ATCC 600703, *Enterococcus faecalis* ATCC 29212, *Staphylococcus aureus* ATCC 29213 and *Pseudomonas aeruginosa* ATCC 27853 using the agar disk diffusion method. Bacterial strains were obtained from the American Type Culture Collection (ATCC, Manassas, VA, USA). β-CD/HEMA was also tested as a reference. Briefly, empty cryogel disks (3 mg) loaded with 10 μg of the antibiotic Lomefloxacin (Sigma-Aldrich, L2906) were placed on Mueller–Hinton agar Oxoid™ (Thermo Scientific™, CM0337B) plates pre-inoculated with the previously listed pathogens. A disk of Lomefloxacin Oxoid™ 10 μg (Thermo Scientific™, CT1661B) was used as an internal control. The plates were incubated at 37 °C overnight aerobically, and the inhibition zones were then measured in mm using a caliper. Furthermore, antibacterial activity against *S. aureus*, *P. aeruginosa*, and *K. pneumoniae* strains was also studied using broth dilution. Minimum inhibitory concentration (MIC) was determined as previously described.[34] Briefly, a bacterial suspension of 0.5 McFarland (equal to 1.5×10^8 CFU mL^{-1}) was made for each strain under examination, and subsequent dilutions in Mueller–Hinton broth Oxoid™ (Thermo Scientific™, CM0405B) were prepared to obtain a final concentration of 10^4 CFU mL^{-1} in the plate. β-cyclodextrin-maltol formulation was added in a concentration range from 1.5 mg to 12.0 mg. Each plate was prepared by including a positive control for bacterial growth (C+) and a negative sterility control for the medium Mueller–Hinton (C−). Inoculated plates were incubated aerobically with shaking at 37 °C for 24 hours, and OD600 measurements (BioTek Microplate Reader – Synergy HTX) were made every 30 minutes. All measurements were repeated six different times. The day after, to assess whether the activity of compound **8** was bactericidal or bacteriostatic, 10 μL of each bacterial culture from the plates with no observable growth were added to MH agar plates and incubated at 37 °C for 24 hours. The presence of viable bacteria was examined on the plate to identify the lowest concentration without observable viable bacteria, designated as the minimum bactericidal concentration (MBC). Each formulation was tested six times against each bacterial strain; the same experiment was repeated on a different day to ensure reproducibility.

Cell cultures and cell viability assay

H1HeLa CRL-1958™ cells were obtained from the American Type Culture Collection (Manassas, VA, USA). Cell lines were maintained in Leibovitz's ʟ-15 medium containing 2 mM ʟ-glutamine, supplemented with 10% fetal bovine serum (FBS) and with 100 U mL^{-1} penicillin and 100 μg mL^{-1} streptomycin in a humidified incubator at 37 °C providing 5% CO$_2$. Cell viability was assessed using the 3-[4,5-dimethyl thiazol-2-yl]-2,5-diphenyl tetrazolium bromide (MTT) assay as previously described.[35] Briefly, cells were seeded in 96-well plates at 1×10^3 cells per well. After 24 h of treatment with 3.0 mg of cryogel, MTT solution (5 mg mL^{-1}) was added to each well. After 3 h of incubation, formazan crystals were dissolved in 150 μL of 0.1 M HCl in isopropanol. The color intensity was measured at 570 nm (BioTek Microplate Reader - Synergy HTX).

Conclusions

Antibiotic resistance is a pressing global health concern, characterized by bacteria's ability to adapt and survive exposure to antibiotics, making these life-saving drugs less effective or ineffective. It is essential to explore novel therapeutic agents or treatment strategies that can enhance medication delivery and enable the implementation of localized antimicrobial therapy.

Remarkable efforts have been made to build nanocontainer systems to release specific drugs by changing the lumen dimensions, charge, hydrophilic/hydrophobic balance, and surface properties.[36] In this context, hydrogels and cryogels have recently received attention in the biomedical area. Compared to others reported in the literature, the advantage of these systems is that they offer a versatile and effective solution for promoting wound healing. They provide the conditions and functionality for optimal recovery (adequate adhesion, secretion absorption, oxygen delivery, hemostasis, tissue regeneration, and re-epithelialization during wound healing). The game changer proposed herein entails the intrinsic antibacterial activity of our product. To the best of our knowledge, this maltol-based cryogel is innovative regarding material and action process. It ensures an eco-friendly bactericidal effect without using external stimuli,[37] nanoparticles,[38] chemicals,[39] or pharmaceuticals.[40] The latter can constitute emerging contaminants when released in the surrounding water environment. It contains 25% maltol and 25% β-cyclodextrin cavities covalently bonded to the material, which can cover additional antibiotic supply if needed. We successfully tested it by using LOM. This finding may open a new vista for future research and applications for infection treatment, *e.g.*, using **8** with pharmaceuticals (antibiotics or others), a revaluation or amplification of their effects can be promoted.

Conflicts of interest

There are no conflicts to declare.

Acknowledgements

European Union nor the European Commission can be held responsible for them.

References

1 M. Saha and A. Sarkar, *J. Xenobiot.*, 2021, **11**, 197–214.

2 A. L. Santos, C. L. Sodre, R. S. Valle, B. A. Silva, E. A. Abi-Chacra, L. V. Silva, A. L. Souza-Goncalves, L. S. Sangenito, D. S. Goncalves, L. O. Souza, V. F. Palmeira, C. M. d'Avila-Levy, L. F. Kneipp, A. Kellett, M. McCann and M. H. Branquinha, *Curr. Med. Chem.*, 2012, **19**, 2715–2737.

3 S. Ghanem, C. J. Kim, D. Dutta, M. Salifu and S. H. Lim, *J. Intern. Med.*, 2021, **290**, 40–56.

4 D. Simoes, S. P. Miguel, M. P. Ribeiro, P. Coutinho, A. G. Mendonca and I. J. Correia, *Eur. J. Pharm. Biopharm.*, 2018, **127**, 130–141.

5 D. Repac Antić, M. Parčina, I. Gobin and M. Petković Didović, *Antibiotics*, 2022, **11**, 1105.

6 N. K. Boyd, C. Teng and C. R. Frei, *Front. Cell. Infect. Microbiol.*, 2021, **11**, 684515.

7 X. Fang, C. Wang, S. Zhou, P. Cui, H. Hu, X. Ni, P. Jiang and J. Wang, *Gels*, 2022, **8**, 315.

8 C. Zagni, A. Coco, V. Patamia, G. Floresta, G. Curcuruto, K. Mangano, T. Mecca, A. Rescifina and S. Carroccio, *Med. Sci. Forum.*, 2022, **14**, 150.

9 C. Zagni, S. Dattilo, T. Mecca, C. Gugliuzzo, A. A. Scamporrino, V. Privitera, R. Puglisi and S. Carola Carroccio, *Eur. Polym. J.*, 2022, **179**, 111556.

10 M. Wang, X. Huang, H. Zheng, Y. Tang, K. Zeng, L. Shao and L. Li, *J. Controlled Release*, 2021, **337**, 236–247.

11 M. H. Norahan, S. C. Pedroza-González, M. G. Sánchez-Salazar, M. M. Álvarez and G. Trujillo de Santiago, *Bioact. Mater.*, 2023, **24**, 197–235.

12 E. Caló and V. V. Khutoryanskiy, *Eur. Polym. J.*, 2015, **65**, 252–267.

13 Y. Liang, J. He and B. Guo, *ACS Nano*, 2021, **15**, 12687–12722.

14 L. Nie, Q. Wei, J. Li, Y. Deng, X. He, X. Gao, X. Ma, S. Liu, Y. Sun, G. Jiang, O. V. Okoro, A. Shavandi and S. Jing, *RSC Adv.*, 2023, **13**, 8502–8522.

15 J. J. Rice, M. M. Martino, L. De Laporte, F. Tortelli, P. S. Briquez and J. A. Hubbell, *Adv. Healthcare Mater.*, 2013, **2**, 57–71.

16 C. Zagni, A. A. Scamporrino, P. M. Riccobene, G. Floresta, V. Patamia, A. Rescifina and S. C. Carroccio, *Nanomaterials*, 2023, **13**, 741.

17 S. Sagbas, N. Aktas and N. Sahiner, *Appl. Surf. Sci.*, 2015, **354**, 306–313.

18 S. Diken Gür, M. Bakhshpour, N. Bereli and A. Denizli, *J. Biomat. Sci., Polym. Ed.*, 2021, **32**, 1024–1039.

19 C. Zagni, A. Coco, T. Mecca, G. Curcuruto, V. Patamia, K. Mangano, A. Rescifina and S. C. Carroccio, *Mater. Chem. Front.*, 2023, **7**, 2693–2705.

20 S. Bhat, A. Tripathi and A. Kumar, *J. R. Soc., Interface*, 2011, **8**, 540–554.

21 M. A. Barrand, B. A. Callingham and R. C. Hider, *J. Pharm. Pharmacol.*, 1987, **39**, 203–211.

22 Z. D. Liu, S. Piyamongkol, D. Y. Liu, H. H. Khodr, S. L. Lu and R. C. Hider, *Bioorg. Med. Chem.*, 2001, **9**, 563–573.

23 A. Synytsya, P. Blafková, A. Synytsya, J. Čopíková, J. Spěváček and M. Uher, *Carbohydr. Polym.*, 2008, **72**, 21–31.

24 J. J. Faig, A. Moretti, L. B. Joseph, Y. Zhang, M. J. Nova, K. Smith and K. E. Uhrich, *Biomacromolecules*, 2017, **18**, 363–373.

25 V. Patamia, R. Tomarchio, R. Fiorenza, C. Zagni, S. Scirè, G. Floresta and A. Rescifina, *Catalyst*, 2023, **13**, 41.

26 S. T. Koshy, D. K. Y. Zhang, J. M. Grolman, A. G. Stafford and D. J. Mooney, *Acta Biomater.*, 2018, **65**, 36–43.

27 E. Amata, N. D. Bland, C. T. Hoyt, L. Settimo, R. K. Campbell and M. P. Pollastri, *Bioorg. Med. Chem. Lett.*, 2014, **24**, 4084–4089.

28 C. Zagni, A. Coco, S. Dattilo, V. Patamia, G. Floresta, R. Fiorenza, G. Curcuruto, T. Mecca and A. Rescifina, *Mater. Today Chem.*, 2023, **33**, 101715.

29 J. Siepmann and F. Siepmann, *Int. J. Pharm.*, 2013, **453**, 12–24.

30 S. Khan and N. M. Ranjha, *Polym. Bull.*, 2014, **71**, 2133–2158.

31 N. A. Peppas, *Pharm. Acta. Helv.*, 1985, **60**, 110–111.

32 D. R. Paul, *Int. J. Pharm.*, 2011, **418**, 13–17.

33 C. Corsaro, G. Neri, A. M. Mezzasalma and E. Fazio, *Polymers*, 2021, **13**, 2897.

34 V. Patamia, C. Zagni, R. Fiorenza, V. Fuochi, S. Dattilo, P. M. Riccobene, P. M. Furneri, G. Floresta and A. Rescifina, *Nanomaterials*, 2023, **13**, 2036.

35 V. Fuochi, I. Barbagallo, A. Distefano, F. Puglisi, R. Palmeri, M. Di Rosa, C. Giallongo, L. Longhitano, P. Fontana, G. Sferrazzo, F. Tiralongo, S. A. Raccuia, S. Ronsisvalle, G. Li Volti, P. M. Furneri and D. Tibullo, *Eur. Rev. Med. Pharmacol. Sci.*, 2019, **23**, 2280–2292.

36 M. C. Scicluna and L. Vella-Zarb, *ACS Appl. Nano Mater.*, 2020, **3**, 3097–3115.

37 S. Liu, H. Yuan, H. Bai, P. Zhang, F. Lv, L. Liu, Z. Dai, J. Bao and S. Wang, *J. Am. Chem. Soc.*, 2018, **140**, 2284–2291.

38 N. A. Ismail, K. A. M. Amin, F. A. A. Majid and M. H. Razali, *Mater. Sci. Eng., C*, 2019, **103**, 109770.

39 S. Li, N. Jiang, W. Zhao, Y.-F. Ding, Y. Zheng, L.-H. Wang, J. Zheng and R. Wang, *Chem. Commun.*, 2017, **53**, 5870–5873.

40 E. Gámez-Herrera, S. García-Salinas, S. Salido, M. Sancho-Albero, V. Andreu, M. Pérez, L. Luján, S. Irusta, M. Arruebo and G. Mendoza, *Eur. J. Pharm. Biopharm.*, 2020, **152**, 327–339.